C1q/TNF-related protein 2 (CTRP2) deletion promotes adipose tissue lipolysis and hepatic triglyceride secretion

Received for publication, May 6, 2019, and in revised form, August 16, 2019 Published, Papers in Press, August 22, 2019, DOI 10.1074/jbc.RA119.009230

Xia Lei[1] **and G. William Wong**[2]

From the Department of Physiology and Center for Metabolism and Obesity Research, School of Medicine, The Johns Hopkins University, Baltimore, Maryland 21205

Edited by Jeffrey E. Pessin

The highly conserved C1q/TNF-related protein (CTRP) family of secreted hormones has emerged as important regulators of insulin action and of sugar and fat metabolisms. Among these, the specific biological function of CTRP2 remains elusive. Here, we show that the expression of human *CTRP2* is positively correlated with body mass index (BMI) and is up-regulated in obesity. We used a knockout (KO) mouse model to determine CTRP2 function and found that *Ctrp2*-KO mice have significantly elevated metabolic rates and energy expenditure leading to lower body weights and lower adiposity. CTRP2 deficiency up-regulated the expression of lipolytic enzymes and protein kinase A signaling, resulting in enhanced adipose tissue lipolysis. In cultured adipocytes, CTRP2 treatment suppressed triglyceride (TG) hydrolysis, and its deficiency enhanced agonist-induced lipolysis *in vivo*. CTRP2-deficient mice also had altered hepatic and plasma lipid profiles. Liver size and hepatic TG content were significantly reduced, but plasma TG was elevated in KO mice. Both plasma and hepatic cholesterol levels, however, were reduced in KO mice. Loss of CTRP2 also enhanced hepatic TG secretion and contributed to impaired plasma lipid clearance following an oral lipid gavage. Liver metabolomic analysis revealed significant changes in diacylglycerols and phospholipids, suggesting that increased membrane remodeling may underlie the altered hepatic TG secretion we observed. Our results provide the first *in vivo* evidence that CTRP2 regulates lipid metabolism in adipose tissue and liver.

The global rise in obesity and associated comorbidities has sparked intense efforts to understand adipocyte biology (1, 2). White adipose tissue serves critical conserved functions as the major storage depot for excess fat and as a major source of numerous secretory proteins and hormones, collectively termed adipokines (3). Many of these adipokines (*e.g.* adiponectin, leptin, omentin, resistin, and RBP4) have endocrine roles in regulating food intake, sugar and fat metabolism, vascular homeostasis, and immune responses (4, 5). The circulating levels of many adipokines are frequently dysregulated in the context of obesity and diabetes (6).

Our recent efforts to better understand tissue crosstalk and endocrine control of metabolism led to the identification and characterization of a highly conserved family of secreted plasma proteins known as the C1q/TNF-related proteins (CTRP1–15) (7–13). Both adiponectin and the CTRPs are part of the larger C1q family, currently comprising >30 members, each encoded by a distinct gene. All share a structurally homologous C-terminal globular C1q domain (14, 15). Each of the CTRP proteins has a distinct tissue expression profile and a few are highly expressed in adipose tissue (14). Genetic gain- and loss-of-function mouse models indicate overlapping and non-redundant metabolic functions for the C1q family members that have been characterized thus far (7, 8, 16–29).

Mouse *Ctrp2* transcript is enriched in adipose tissue (12) and CTRP2 is mainly produced by stromal vascular compartment cells in adipose tissue. Its expression in adipose tissue is up-regulated in leptin-deficient (*ob/ob*) obese mice relative to lean controls (12). Of the C1q family members, CTRP2 shares one of the highest degrees of amino acid identity (43%) with adiponectin in the globular C1q domain. We previously showed that mouse CTRP2 can activate AMP-activated protein kinase (AMPK) and increase glycogen deposition and fat oxidation in cultured C2C12 myotubes (13). In a transgenic mouse model with elevated circulating plasma CTRP2, we observed an enhanced rate of lipid clearance from circulation following an acute lipid infusion (30). The level of locally produced CTRP2 in skeletal muscle is also elevated in aged rats (24 months old) compared with young rats (4 months old) (31). Aside from these limited studies, the biological function of CTRP2 in a normal physiological context is unknown.

To decipher the function and mechanisms of action of endogenous CTRP2, we used a genetic loss-of-function mouse model. This study provides the first evidence that CTRP2 is indeed a secreted regulator of lipid metabolism *in vivo* and is required for maintaining energy homeostasis.

Results

Increased adipose expression of CTRP2 in human obesity

Sequence alignments indicate a high degree of amino acid identity (94%) between full-length human and mouse CTRP2

This work was supported by National Institutes of Health Grant DK084171 (to G. W. W.). The authors declare that they have no conflicts of interest with the contents of this article. The content is solely the responsibility of the authors and does not necessarily represent the official views of the National Institutes of Health.

[1] Recipient of American Heart Association postdoctoral fellowship POST17070119. To whom correspondence may be addressed: Dept. of Biochemistry and Molecular Biology, Oklahoma State University, Stillwater, OK 74078. Tel: 410-502-4862; Fax: 410-614-8033; E-mail: xia.lei@okstate.edu.

[2] To whom correspondence may be addressed. Tel: 410-502-4862; Fax: 410-614-8033; E-mail: gwwong@jhmi.edu.

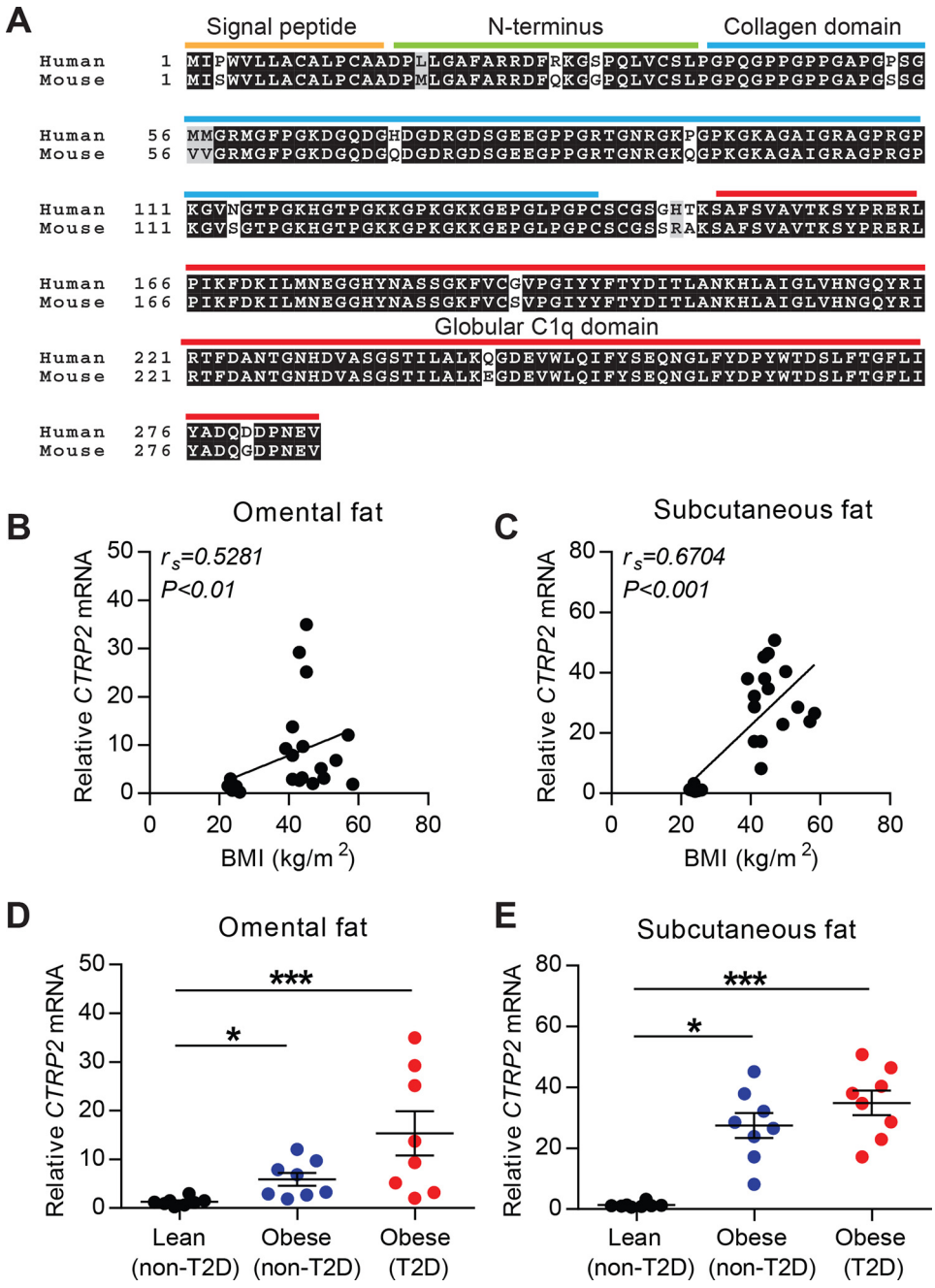

Figure 1. CTRP2 is highly conserved between mice and humans and is up-regulated in human obesity. *A*, sequence alignment of human (NP_114114) and mouse (NP_081255) CTRP2 using a web-based Clustal Omega tool. Identical amino acids are shaded *black* and similar amino acids are shaded *gray*. Shading was done using the web-based BoxShade tool. The signal peptide, N terminus, collagen domain, and globular C1q domain are indicated. *B–E*, real-time PCR analysis of *CTRP2* expression in visceral (omental) and subcutaneous white adipose tissue of human abdominal surgery subjects. Expression of *CTRP2* in both fat depots is positively correlated with BMI (*B* and *C*). Expression of *CTRP2* in both fat depots is significantly increased in obese patients with or without type 2 diabetes relative to healthy lean controls without type 2 diabetes (*D* and *E*). $n = 8$/group. Expression levels were normalized to *36B4* (also known as *RPLP0*) in each sample. *, $p < 0.05$; ***, $p < 0.001$. *Error bars*, S.E.

protein (Fig. 1*A*), suggesting conserved structure and function. We previously showed that *Ctrp2* mRNA expression in visceral adipose tissue was significantly increased in C57BL/6J male mice fed a high-fat diet (HFD)[3] for 12 weeks compared with mice fed a control low-fat diet (LFD) (30). To address whether adipose expression of *CTRP2* is also altered in human obesity, we measured its mRNA levels in visceral (omental) and subcutaneous fat depots obtained from healthy lean controls as well as obese individuals with and without type 2 diabetes. Expres-

[3] The abbreviations used are: HFD, high-fat diet; BMI, body mass index; BW, body weight; EE, energy expenditure; eWAT, epididymal white adipose tissue; GTT, glucose tolerance tests; HDL, high-density lipoprotein; ITT, insulin tolerance tests; iWAT, inguinal white adipose tissue; LDL, low-density lipoprotein; LFD, low-fat diet; LPL, lipoprotein lipase; OFTT, oral fat tolerance tests; PC, phosphatidylcholines; PE, phosphatidylethanolamines; RER, respiratory exchange ratio; T2D, type 2 diabetes; TG, triglyceride; TNF, tumor necrosis factor; VLDL, very low-density lipoprotein.

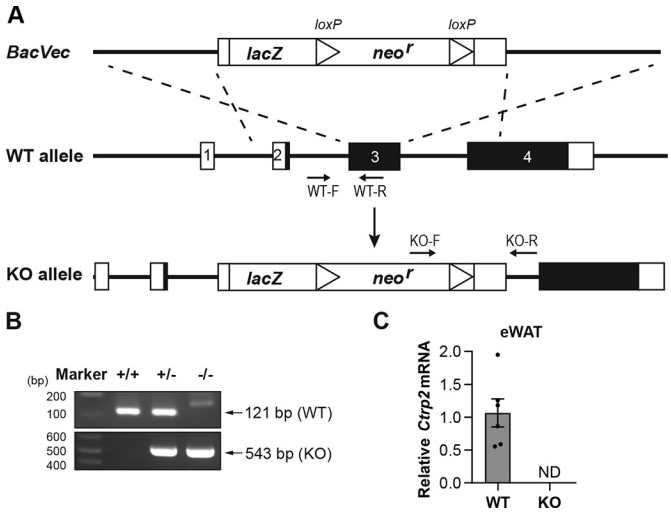

Figure 2. *Ctrp2* KO mouse model. *A*, schematic showing the gene targeting strategy used to generate *Ctrp2* KO mice. *B*, PCR genotyping results showing the successful generation of WT (+/+), heterozygous (+/−), and homozygous (−/−) knock-out mice using the indicated primer pairs as shown in *A*. *C*, the absence of *Ctrp2* mRNA in eWAT of KO mice was confirmed by real-time PCR using primer pairs specific for *Ctrp2*. Expression levels were normalized to *β-actin* in each sample. WT, $n = 6$; KO, $n = 8$. *ND*, not detected. *Errors bars* represent Mean ± S.E.

sion of *CTRP2* in both omental and subcutaneous fat depots was positively correlated with body mass index (BMI) in humans (Fig. 1, *B* and *C*). Compared with lean controls, *CTRP2* expression was markedly up-regulated in both the omental and subcutaneous fat depots of obese individuals with and without type 2 diabetes (Fig. 1, *D* and *E*).

Reduced body weight and increased energy expenditure in LFD- and HFD-fed Ctrp2 knockout mice

A genetic loss-of-function mouse model was used to determine the metabolic role of CTRP2 *in vivo* (Fig. 2*A*). Two sets of primers were designed to amplify a sequence spanning intron 2 and exon 3 of the WT allele and a sequence spanning the downstream deletion site in the *lacZ* gene to confirm the genotype of WT and KO mice, respectively (Fig. 2*B*). As expected from targeted disruption of the gene, *Ctrp2* mRNA was absent from the epididymal white adipose tissue (eWAT) of KO mice (Fig. 2*C*). *Ctrp2* KO mice were born at the expected Mendelian ratio and appeared normal with no gross developmental abnormalities. Although *Ctrp2* mRNA is expressed at low levels during embryonic development (12), its deletion is dispensable for mouse development.

To determine the contribution of CTRP2 to systemic energy metabolism in the normal and obese states, WT and *Ctrp2* KO male and female mice were fed an HFD or a control LFD for 16 weeks, beginning at 5 weeks of age. In both LFD- and HFD-fed groups, we observed reduced body weight in male KO mice compared with WT littermates. However, there were no differences between female WT and KO mice on either diet (Fig. 3, *A* and *B*). For this reason, we chose to focus our metabolic analyses on male mice. In the LFD-fed group, *Ctrp2* KO mice showed reduced whole-body fat mass accounting for the reduced body weight relative to WT littermates. However, in the HFD-fed group, reduced body weight of KO mice was because of a significant reduction in both fat and lean mass (Fig. 3*C*). No differences in food intake or total physical activity were seen between genotypes (Fig. 3, *D* and *E*). However, elevated metabolic rate, indicated by reduced respiratory exchange ratio (RER) and reflected by increased oxygen consumption rate ($\dot{V}_{O2}$) and increased fat oxidation, were observed in LFD-fed KO mice (Fig. 3, *F* and *H*). In contrast, increased CO_2 production rate ($\dot{V}_{CO2}$) was only seen in HFD-fed KO mice (Fig. 3*G*). Accordingly, both LFD- and HFD-fed KO mice had significantly increased energy expenditure, and the effect was much more pronounced in the LFD-fed KO mice (Fig. 3, *I* and *J*). For this reason, we focused our functional studies on LFD-fed mice.

Reduced adiposity and enhanced lipolysis in LFD-fed Ctrp2 KO mice

Consistent with the Echo-MRI results, the weight and size of visceral (eWAT) and subcutaneous (iWAT) fat depots were markedly reduced in *Ctrp2* KO male mice relative to WT littermates (Fig. 4, *A–D*). Histological evaluation of adipocyte morphology in eWAT showed no significant differences between genotypes (Fig. 4*E*). To determine whether altered lipolysis contributes to reduced adipose tissue weight, we examined the three key enzymes (ATGL, HSL, MGL) involved in triglyceride hydrolysis (32) in the fasted states, in which tissues were collected after food was removed for 4 h. Both mRNA and protein expression of these enzymes were significantly up-regulated in the KO mice (Fig. 4, *F–H*). In addition, phosphorylation of PKA substrates were also strikingly elevated in the KO mice, implicating enhanced PKA signaling in promoting adipose tissue lipolysis (Fig. 4*I*). Next, we tested whether stimulated *in vivo* lipolysis in response to β_3-adregenic receptor agonist (CL316243) was also elevated in the KO mice. Plasma free fatty acid (FFA) and glycerol levels were induced by CL316243 to a significantly greater extent in KO mice than in WT controls (Fig. 4, *J* and *K*). In differentiated 3T3-L1 adipocytes, forskolin can robustly increase cAMP accumulation and promote lipolysis (33). To test whether CTRP2 has a direct effect on forskolin-stimulated lipolysis, different concentrations of purified recombinant mouse CTRP2 protein were used to treat differentiated 3T3-L1 adipocytes. Both 5 μg/ml and 10 μg/ml of CTRP2 markedly suppressed adipocyte lipolysis in response to forskolin (Fig. 4*L*). Together, these results support a role for CTRP2 in regulating adipose tissue lipolysis *in vitro* and *in vivo*. In contrast to lipid metabolism, whole-body glucose metabolism was not appreciably affected by CTRP2 deficiency when mice were fed a control LFD; neither glucose nor insulin tolerance test results were different between genotypes (Fig. 4, *M* and *N*).

Altered hepatic and plasma lipid profiles in LFD-fed Ctrp2 KO mice

In the fasted state, plasma triglyceride (TG) levels were significantly higher in KO mice compared with WT littermates, and the TG content of very low-density lipoprotein (VLDL) particles was ~1.8-fold greater in the KO mice (Fig. 5, *A* and *B*). No differences in fecal TG content were noted between genotypes (Fig. 5*C*), indicating that elevated plasma TG levels could not be because of reduced fecal TG excretion. Although plasma

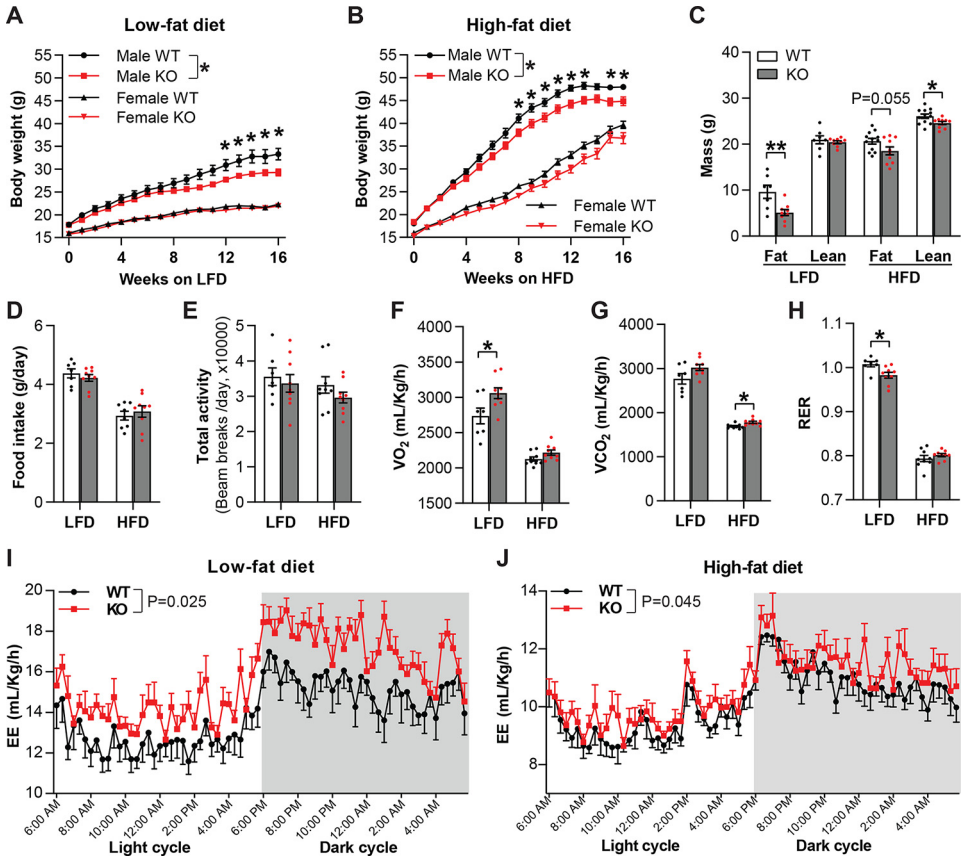

Figure 3. Reduced body weight and increased energy expenditure in both LFD- and HFD-fed *Ctrp2* KO mice. *A* and *B*, body weight of WT and KO male and female mice fed either an LFD or an HFD over time. *C*, total fat and lean mass in WT and KO male mice quantified by NMR (Echo-MRI) at 18 weeks of age. *D–J*, food intake, total physical activity, oxygen consumption rate ($\dot{V}_{O2}$), CO_2 production rate ($\dot{V}_{CO2}$), RER, and EE were measured by CLAMS for WT and KO male mice (20 weeks of age). LFD: male WT, $n = 7$; male KO, $n = 9$; female WT, $n = 9$; female KO, $n = 10$. HFD: male WT, $n = 12$; male KO, $n = 10$; female WT, $n = 9$; female KO, $n = 8$. *, $p < 0.05$; **, $p < 0.01$. For EE (*I* and *J*), in the LFD and HFD groups, WT *versus* KO $p < 0.05$. *Error bars*, S.E.

TG concentration was much higher, total plasma cholesterol was significantly reduced in KO mice (Fig. 5*D*). Cholesterol content was strikingly reduced in the low-density lipoprotein (LDL) and high-density lipoprotein (HDL) particle fractions (Fig. 5*E*). Fecal cholesterol content was also reduced, excluding fecal excretion as a cause of reduced plasma cholesterol levels (Fig. 5*F*). In striking contrast to the plasma lipid profile, the size of the mouse livers and hepatic TG content were both markedly reduced in *Ctrp2* KO mice (Fig. 5, *G–J*). Parallel to the reduction in plasma cholesterol, we also observed reduced hepatic cholesterol content in KO mice (Fig. 5*K*). In striking contrast to eWAT, the expression of lipolytic genes (*Atgl, Hsl, Mgl*) in liver was not different between WT and KO mice (Fig. 5*L*).

To better understand the altered TG metabolism observed in the KO mice, we performed oral fat tolerance tests (OFTT) on overnight-fasted mice to determine whether loss of CTRP2 impairs the ability of the mice to handle an acute lipid load. Following an oral lipid gavage, the *Ctrp2* KO mice had a dramatic rise in serum TG compared with WT controls (Fig. 6*A*). When we administered lipid emulsion via intraperitoneal injection to bypass gut absorption, we still observed a significant increase in serum TG levels at 2 h post injection in the KO mice relative to WT controls (Fig. 6*B*), indicating that increased plasma TG following an acute lipid load is because of elevated hepatic VLDL-TG secretion or reduced lipid clearance from circulation by peripheral tissues. To test the former, we inhibited TG clearance from circulation in fasted mice by administering the nonionic surfactant poloxamer 407, an inhibitor of lipoprotein lipase (LPL) that blocks fatty acid uptake by peripheral tissues (34). In this case, circulating TG is mainly derived from VLDL-TG secreted by the liver. When lipid uptake was blocked in the fasted state, hepatic VLDL-TG secretion was significantly elevated in KO mice (Fig. 6*C*). LPL localized to the luminal surface of vascular endothelial cells is responsible for the bulk of TG clearance from circulation by hydrolyzing circulating TG to release FFAs for use in peripheral tissues. Heparin can be used to displace LPL from the vascular endothelium in mice and LPL activity can then be measured in post-heparin plasma. The postheparin plasma LPL activity was not significantly different between WT and KO mice (Fig. 6*D*). These experiments indicate that enhanced hepatic VLDL-TG secretion contributes to the marked increase in plasma TG levels in KO mice following an acute lipid load.

Increased hepatic membrane remodeling in LFD-fed Ctrp2 KO mice

To further examine alterations of metabolic pathways in the KO mouse liver, we performed unbiased metabolite profiling. In general, phospholipids, including phosphatidylcholines (PC) and phosphatidylethanolamines (PE), were significantly elevated, indicating increased phospholipid synthesis in the liver of KO mice (Fig. 7, *A* and *B*). Multiple intermediates of phos-

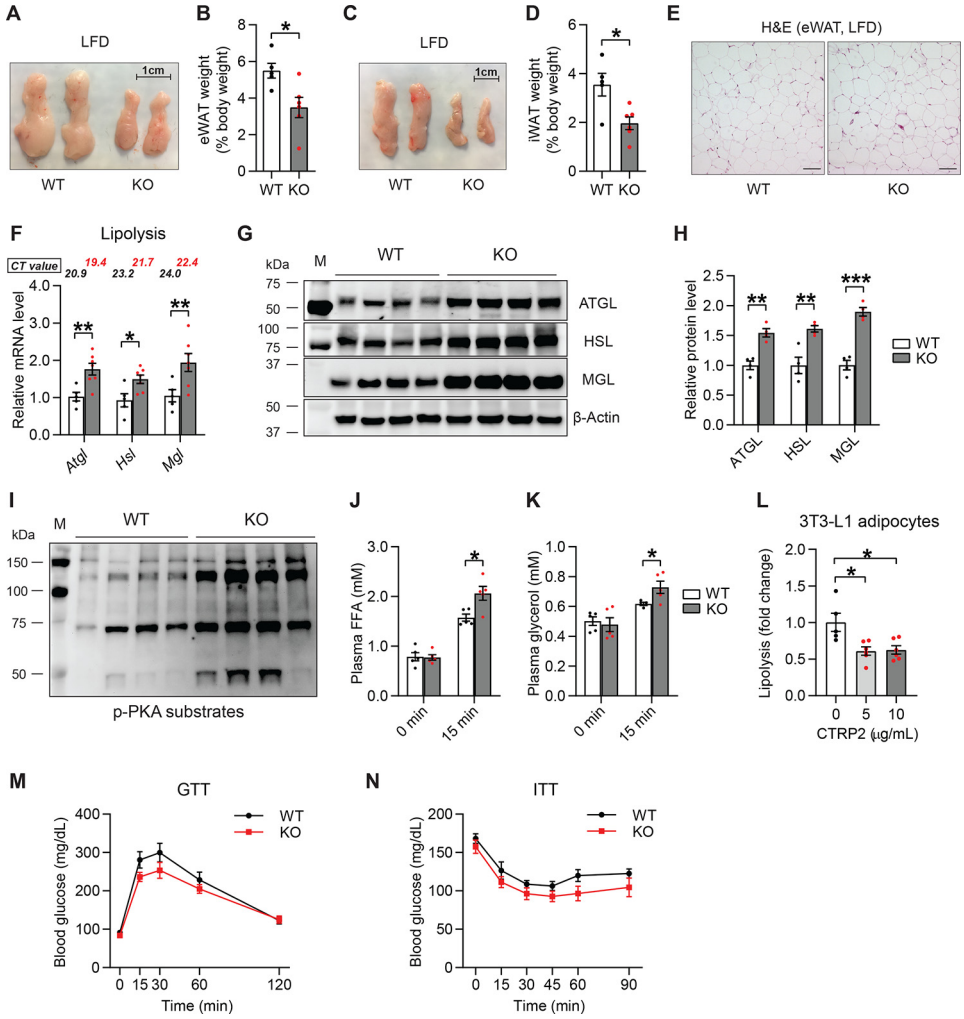

Figure 4. Reduced adiposity and enhanced lipolysis in LFD-fed *Ctrp2* KO male mice. *A–D*, weight of white adipose tissue (eWAT and iWAT; % body weight) in WT and KO mice fed LFD. WT, $n = 6$; KO, $n = 8$. Representative photos of tissues are shown. *E*, representative H&E-stained eWAT from WT and KO mice fed an LFD. *Scale bar* = 100 μm. *F*, real-time PCR for lipolytic gene expression (*Atgl, Hsl, Mgl*) from eWAT of WT and KO mice fed an LFD. Expression levels were normalized to *β-actin* in each sample. WT, $n = 6$; KO, $n = 8$. *G*, Western blot analysis of lipolytic enzymes (ATGL, HSL, MGL) from eWAT of WT and KO mice. *H*, quantification of protein expression in KO mice compared with WT mice as shown in (*G*) using ImageJ software. *I*, Western blotting of phospho-PKA substrates from eWAT of WT and KO mice. *J* and *K*, plasma FFA and glycerol levels 15 min post β_3-adrenergic receptor agonist (CL316243) injection ($n = 5$/group). *L*, forskolin-stimulated lipolysis measured in differentiated 3T3-L1 adipocytes after cells were treated with vehicle or different concentrations of purified recombinant mouse CTRP2 protein for 24 h ($n = 6$/group). *M* and *N*, blood glucose levels of WT ($n = 7$) and KO ($n = 9$) mice fed an LFD at the indicated time points during GTT and ITT. *, $p < 0.05$; **, $p < 0.01$; ***, $p < 0.001$. *Error bars*, S.E.

pholipid metabolism, including CMP, cytidine 5′-diphosphocholine, glycerophosphorylcholine, cytidine 5′-diphosphoethanolamine, and glycerophosphoethanolamine, were increased in the livers of *Ctrp2* KO mice (Fig. 7*C*). Numerous diacylglycerols (also a precursor of phospholipids), such as palmitoyl-palmitoyl-glycerol, were significantly reduced in the livers of KO mice, suggesting an increased utilization of these precursors in phospholipid synthesis (Fig. 7*D*). Collectively, these data suggest substantial cell membrane remodeling in the livers of CTRP2-deficient mice (Fig. 7*E*) which may be needed for enhanced VLDL assembly and TG secretion.

Discussion

Our findings provide insight into the biological function of CTRP2, an enigmatic secretory protein highly conserved from fish to human. The expression of *CTRP2* was significantly upregulated in different fat depots of obese individuals relative to healthy lean controls and was positively correlated with BMI. This correlation prompted us to use a genetic mouse model to assess the metabolic role of CTRP2 in a physiological context. It should be noted that our human data are based on limited samples from mostly Caucasian subjects. Further confirmation is needed in a larger cohort of human samples from multiple racial and ethnic groups.

When fed either a control low-fat diet or a high-fat diet, *Ctrp2* KO male mice gained significantly less (~5 g less) body weight relative to WT littermate controls. This body weight phenotype appeared to be sex-dependent, as female mice lacking CTRP2 were indistinguishable from WT littermates regardless of diet, reinforcing the importance of sex as a biological variable contributing to phenotypic outcomes. Reduced body weight and fat mass in male *Ctrp2* KO mice was not because of decreased food intake or increased physical activity; instead, it was attributed to increased metabolic rate and energy expend-

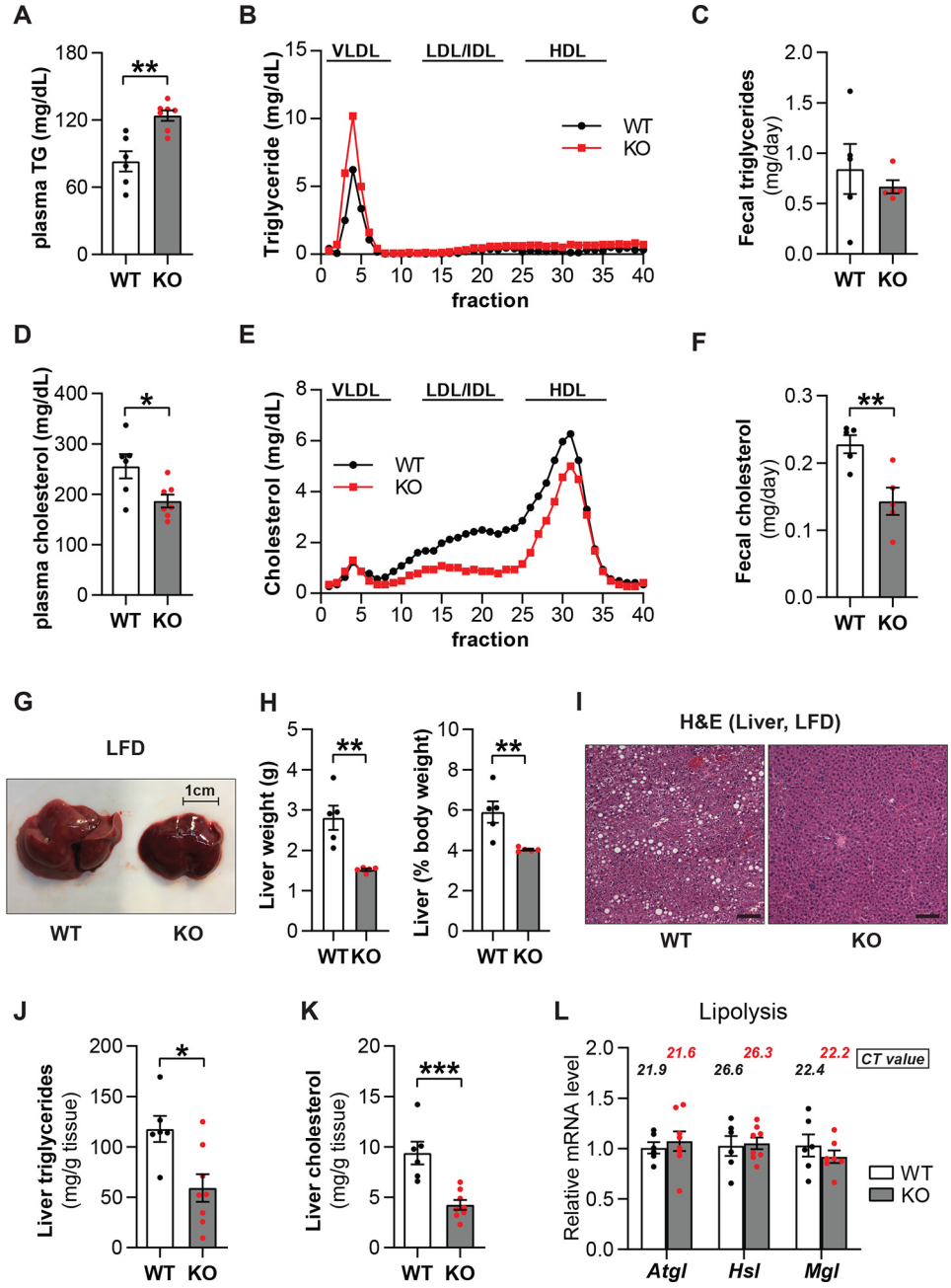

Figure 5. Altered triglyceride and cholesterol levels in plasma, livers, and fecal pellets from LFD-fed *Ctrp2* KO male mice. *A–C*, TG levels in plasma, VLDL, LDL, and HDL separated by FPLC and fecal pellets of WT and KO mice fed an LFD. *D–F*, cholesterol levels in plasma, VLDL, LDL, and HDL separated by FPLC and fecal pellets of WT and KO mice. For plasma, liver, and fecal samples, WT, $n = 6$; KO, $n = 8$. For FPLC, samples were pooled from four mice for each group. *G*, representative liver from WT and KO male mice. *H*, liver wet weight and its percentage of body weight in WT and KO male mice. *I*, representative liver histology (H&E stained) of WT and KO male mice. *Scale bar* = 100 μM. *J* and *K*, liver TG and cholesterol content in WT and KO male mice. *L*, quantitative real-time PCR analysis of lipolytic gene expression (*Atgl*, *Hsl*, *Mgl*) in the livers of WT and KO mice fed an LFD. Expression levels were normalized to *β-actin* in each sample. WT, $n = 6$; KO, $n = 8$. *, $p < 0.05$; **, $p < 0.01$; ***, $p < 0.001$. *Error bars*, S.E.

iture. Male mice lacking CTRP2 also had a lower respiratory exchange ratio, suggesting a preferential use of lipid substrates for oxidative metabolism. Loss of CTRP2 preferentially affected lipid, but not glucose, metabolism. Assessment of whole-body carbohydrate metabolism by glucose and insulin tolerance tests revealed no differences in glucose clearance and insulin sensitivity in *Ctrp2* KO male mice fed a low-fat diet relative to WT littermates.

Several notable lipid phenotypes were observed in the *Ctrp2* KO mice. In the absence of CTRP2, we observed enhanced expression of the major lipolytic enzymes (ATGL, HSL, and MGL) at both the mRNA and protein levels in adipose tissue. Whereas adipose tissue triglyceride lipase (*Atgl*) and hormone-sensitive lipase (*Hsl*) expression are known to be regulated by anti-diabetic drugs, insulin, and stress hormones (*e.g.* glucocorticoids and ACTH) (35–40), much less is known about what signals regulate monoacylglycerol lipase (*Mgl*) expression (41). Thus, the induction of all three lipolytic enzymes in KO mice suggests that CTRP2 may be involved in regulating the expression of these catabolic enzymes in adipose tissue. Mice lacking

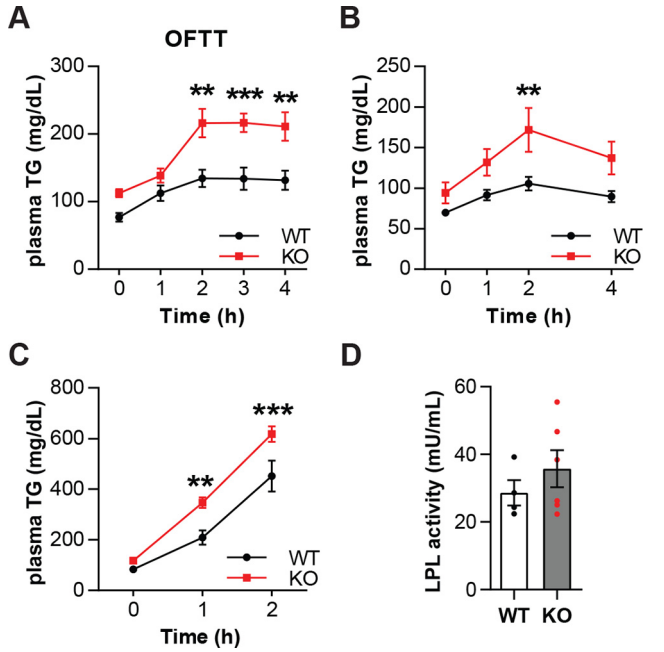

Figure 6. Impaired lipid tolerance in LFD-fed *Ctrp2* KO male mice. *A*, plasma TG levels measured at the indicated time points during OFTT. *B*, plasma TG measured during intraperitoneal fat tolerance test. *C*, plasma TG measured after administration of poloxamer 407 (an inhibitor of lipoprotein lipase activity) in overnight-fasted mice. *D*, LPL activity measured in post-heparin plasma. $n = 6–8$/group. **, $p < 0.01$; ***, $p < 0.001$. *Error bars*, S.E.

CTRP2 also had enhanced PKA signaling. Both increased expression of lipolytic enzymes, and PKA signaling contributed to the elevated adipose tissue lipolysis seen in the *Ctrp2* KO mice in response to β_3-adregenic receptor agonist (CL316243) stimulation. Using cultured 3T3-L1 differentiated adipocytes *in vitro*, we demonstrated a direct role for CTRP2 in regulating TG hydrolysis. Treatment of adipocytes with recombinant CTRP2 robustly suppressed forskolin-induced lipolysis. Thus, our *in vitro* and *in vivo* data suggest that CTRP2 has anti-lipolytic action on adipocytes. In this context, the observed up-regulation of *CTRP2* in obese human adipose tissue may be clinically relevant as obesity-linked insulin resistance promotes adipose tissue lipolysis (42). Interestingly, the related C1q family member adiponectin was also reported to inhibit basal and catecholamine-induced lipolysis in human and mouse adipocytes (43, 44), highlighting a shared biological function between the two related secretory proteins. Reduced fat mass seen in the KO mice could also be because of decreased lipid synthesis and/or increased fat oxidation in the adipose tissue. Assessment of a panel of lipid synthesis and oxidation genes in adipose tissue ruled out these possibilities (data not shown). Thus, lower adiposity in *Ctrp2* KO mice is likely because of the combined effects of increased whole-body energy expenditure and elevated adipose tissue lipolysis.

In the absence of CTRP2, we observed a marked increase in fasting plasma TG and VLDL-TG levels in LFD-fed KO mice. This prompted us to examine whether CTRP2 is required for proper handling of an acute lipid load. We saw a striking impairment of lipid clearance from circulation following an oral lipid gavage in the *Ctrp2* KO mice relative to WT littermates. Changes in plasma TG levels following an oral lipid load are generally attributed to TG associated with chylomicron and nonchylomicron fractions (chylomicron remnants, VLDL, and VLDL remnants) (45, 46). Because fecal TG content was not different between genotypes, we assumed that there was no difference in intestinal fat absorption or chylomicron secretion. Importantly, when we delivered the emulsified lipids via intraperitoneal injection to bypass gut absorption, we still observed significant differences in plasma TG levels in the *Ctrp2* KO mice relative to WT controls. Therefore, increased plasma TG following lipid loading could be because of reduced lipid uptake into peripheral tissues or increased hepatic TG secretion in the form of VLDL-TG particles. LPL plays a critical role in lipid uptake from the circulation by peripheral tissues (47). We observed no differences in post-heparin LPL activity between WT and KO mice. In contrast, when we prevented tissue uptake of circulating TG by inhibiting LPL with poloxamer 407, we observed a marked increase in plasma TG in the *Ctrp2* KO mice. The extent to which plasma TG rises in response to LPL inhibition (in the fasted state) largely reflects hepatic TG secretion in the form of VLDL-TG particles. Combined, our data suggest that CTRP2 modulates VLDL-TG secretion and that its absence promotes hepatic TG secretion leading to the elevated plasma TG and VLDL-TG seen in the KO mice.

Unlike the reciprocal changes in plasma and liver TG content, cholesterol levels in both liver and plasma were significantly reduced in *Ctrp2* KO mice fed either a control low-fat diet or a high-fat diet. In mice, cholesterol turnover involved 1) cholesterol synthesis in hepatic and extrahepatic tissues, 2) cholesterol transport in plasma and uptake via LDL and HDL receptors, and 3) cholesterol excretion from the liver into the intestine in the form of bile acids (48). In LFD-fed mice, lower plasma cholesterol levels in KO mice were attributed to lower LDL-cholesterol and HDL-cholesterol. Because fecal cholesterol was significantly reduced in KO mice, this ruled out enhanced bile acid excretion as a cause of lower plasma cholesterol. Our data suggest that reduced hepatic cholesterol synthesis likely accounts, at least in part, for the lower plasma and liver cholesterol observed in the *Ctrp2* KO mice. Alternatively, this phenotype could be because of reduced cholesterol uptake by the intestine in *Ctrp2* KO mice.

Hepatic VLDL assembly and secretion can be significantly altered by *de novo* biosynthesis of phospholipids, such as PE and PC (49). PC is the major phospholipid component of VLDL and is located on the hydrophilic surface of the particles (50). Two pathways are involved in hepatic PC synthesis: 70% of total hepatic PC synthesis is derived from the CDP-choline pathway, whereas the remaining 30% is synthesized through the PE methylation pathway. Inhibiting PC biosynthesis by choline deprivation strongly reduces VLDL secretion in hepatocytes (51). Inhibiting PC synthesis via the PE methylation pathway also impairs the incorporation of lipids into VLDL in hepatocytes (52). In LFD-fed *Ctrp2* KO mice, hepatic PC and PE levels were dramatically increased and diacylglycerol levels were reciprocally reduced. Because diacylglycerols provide the precursors for PE and PC synthesis, their reduction reflects greater consumption by the PC and PE synthesis pathways. Our metabolite profiling data suggest that increased membrane remodeling in

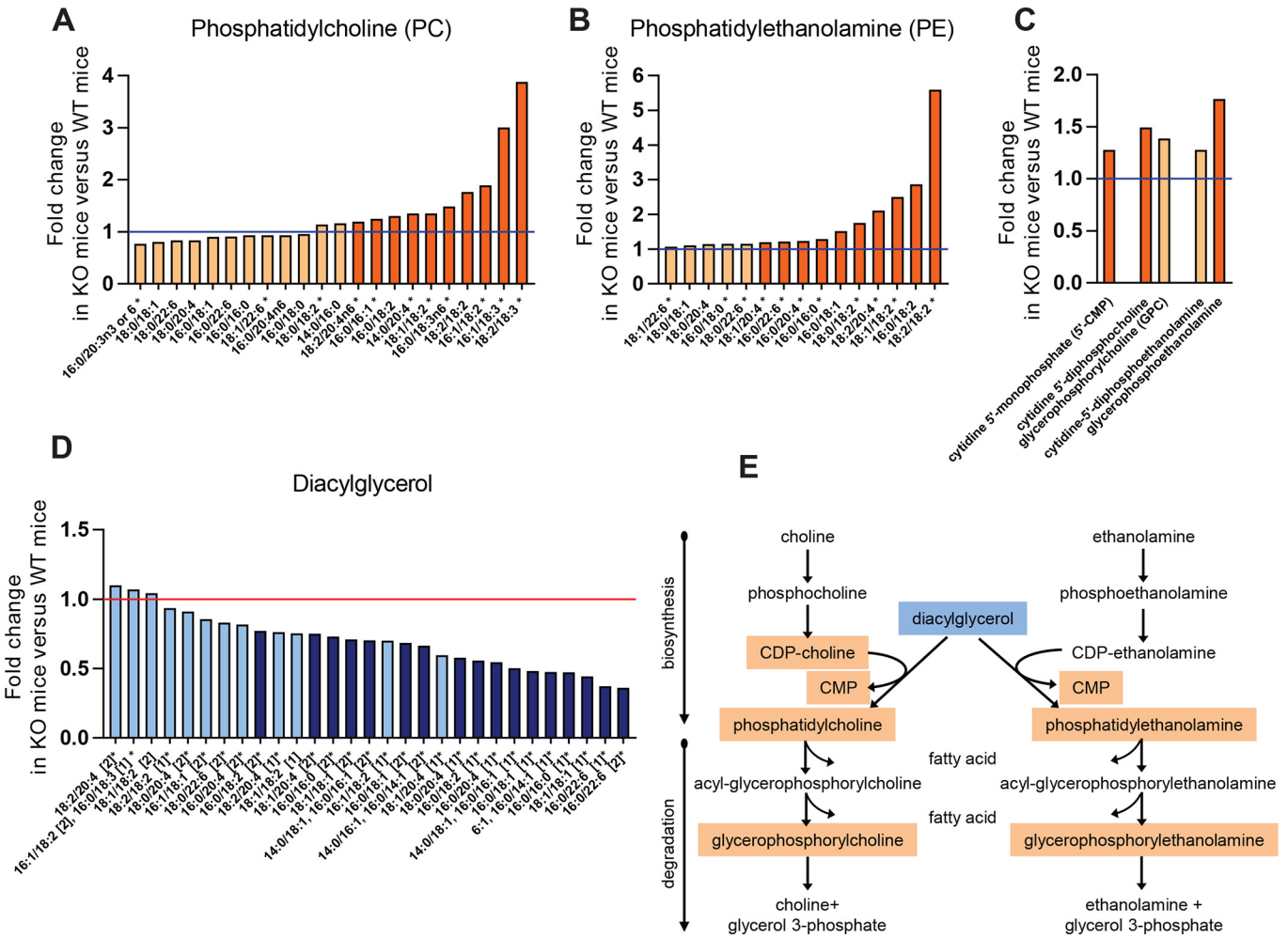

Figure 7. Increased membrane remodeling in LFD-fed *Ctrp2* KO mouse liver. *A* and *B*, -fold change of phosphatidylcholines and phosphatidylethanolamines in liver metabolomic profiles of WT and *Ctrp2* KO mice. *C*, -fold change of phospholipid metabolism intermediates in WT and *Ctrp2* KO mouse liver. *D*, -fold change of diacylglycerols in WT and *Ctrp2* KO mouse liver. The asterisk indicates a compound that has not been confirmed by a standard, but whose identity is known. Biochemical name followed by a number in brackets indicates a compound that is a structural isomer of another compound in the Metabolon spectral library; for example, a diacylglycerol for which more than one stereospecific molecule exists. Bars with *darker colors* indicate statistically significant change. WT, $n = 6$; KO, $n = 8$. *E*, summary of phospholipid metabolic pathways with increased metabolites (*yellow*) and decreased metabolites (*blue*) in *Ctrp2* KO compared with WT mouse liver metabolomic profiles.

hepatocytes likely contributes to the enhanced postprandial VLDL-TG assembly and secretion seen in the *Ctrp2* KO mice.

In summary, our study provides the first *in vivo* evidence that CTRP2 regulates lipid metabolism in adipose tissue and liver either directly or indirectly (Fig. 8). CTRP2 acted on adipocytes to suppress fat mobilization and played a role in restraining excessive TG hydrolysis. Although a direct action on liver still remains to be demonstrated, CTRP2 also appears to affect TG and cholesterol levels in liver, as well as membrane phospholipid turnover, thereby modulating systemic lipid profiles. Future studies will seek to identify the CTRP2 receptor (currently unknown) and signaling pathways engaged by CTRP2 to control fat metabolism in different organs and tissues.

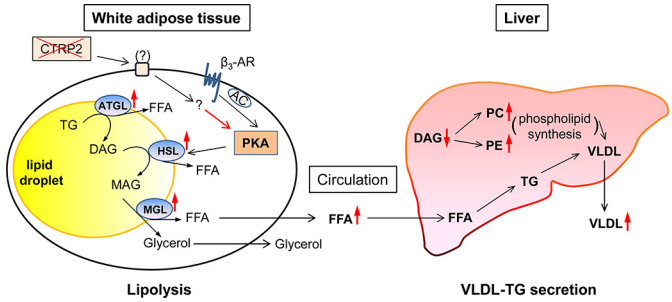

Figure 8. Proposed model of the direct and indirect effects of CTRP2 deficiency on adipose tissue and liver. CTRP2 deficiency stimulates lipolysis in adipose tissue by both activating PKA signaling pathway and up-regulating lipolytic enzymes (ATGL, HSL, MGL) expression. It also promotes TG secretion from liver by increasing phospholipid synthesis, enhancing VLDL assembly and secretion. Although the direct effects of CTRP2 on adipose tissue and adipocytes have been noted, the direct action of CTRP2 on liver still remains to be demonstrated. *β3-AR*, beta-3 adrenergic receptor; *AC*, adenylyl cyclase; *DAG*, diacylglycerol; *MAG*, monoacylglycerol.

Experimental procedures

Human tissue samples

Visceral (omental) and subcutaneous adipose tissues were obtained from the Adipose Biology Core of the National Institutes of Health (NIH)-funded Mid-Atlantic Nutrition Obesity Research Center at the University of Maryland. Study protocols were approved by the Institutional Review Board for Human Subjects Research at the University of Maryland, and the studies abide by the Declaration of Helsinki principles. Written

Table 1
Primers for real-time PCR

Gene	Forward (5′–3′)	Reverse (5′–3′)
Human *CTRP2*	GTATAGACATGCCACGGCGG	GAGGCTAGAACCGCTCACTCG
Human *36B4*	AGCCCAGAACACTGGTCTC	ACTCAGGATTTCAATGGTGCC
Mouse *Ctrp2*	CTGACCCAATGCTTGGTGC	GCCCTTTGGTCCTTGTTTTCC
Mouse *β-Actin*	AGTGTGACGTTGACATCCGTA	GCCAGAGCAGTAATCTCCTTCT
Atgl	TGTGGCCTCATTCCTCCTAC	TCGTGGATGTTGGTGGAGCT
Hsl	GCTGGGCTGTCAAGCACTGT	GTAACTGGGTAGGCTGCCAT
Mgl	CGGACTTCCAAGTTTTTGTCAGA	GCAGCCACTAGGATGGAGATG

informed consent was obtained from all human subjects. Type 2 diabetes (T2D) was determined by hemoglobin A1c values ≥6.5% according to the World Health Organization criteria. Characteristics of the lean controls without type 2 diabetes (non-T2D), obese (non-T2D), and obese with T2D individuals have been described previously (16).

Knockout mouse model

The mouse strain used for this research project, B6;129S5-C1qtnf2-tm1Lex/Mmcd (stock number 032165-UCD), was obtained from the Mutant Mouse Regional Resource Center (MMRRC), a National Center for Research Resources funded strain repository, and was donated to the MMRRC by Genentech, Inc. To generate *Ctrp2* KO mice, the entire exon 3 (260 bp on chromosome 11) was replaced with a targeting cassette containing the β-gal reporter gene, *lacZ*. Genotyping primers for the WT allele were WT-F (5′-CAGTGGAGAAGAAGGTAAGAGACC-3′) and WT-R (5′-TAACAGGTAGTGATGAGTGCTAGC-3′). The expected size of the WT band was 121 bp. Genotyping primers for the KO allele were KO-F (5′-GCAGCGCATCGCCTTCTATC-3′) and KO-R (5′-GATGACTCTTTCAGAACATCC-3′). The expected size of the KO band was 543 bp. The absence of *Ctrp2* mRNA resulting from the *Ctrp2* gene disruption was confirmed by real-time PCR. The primers used to confirm the presence of *Ctrp2* mRNA are listed in Table 1. *Ctrp2* KO mice were initially generated on a mixed (129/Sv × C57BL/6J) genetic background. We backcrossed the mice onto a C57BL/6J genetic background for more than six generations. For each cohort of mice, at least 10 breeding sets (1 heterozygous male and 2 heterozygous female mice) were set up at the same time. Only homozygous KO male and female mice (−/−) and WT littermate (+/+) controls with close dates of birth were used in our experiments. From 5 weeks of age, *Ctrp2* KO and WT male and female mice were fed either a low-fat diet (10% kcal derived from fat, D12450B; Research Diets) or a high-fat diet (60% kcal derived from fat, D12492; Research Diets), and body weights were measured weekly. All mice were housed in polycarbonate cages under a 12:12–h light-dark photocycle and had access to water *ad libitum* throughout the study period. All animal experiments were approved by the Animal Care and Use Committee at the Johns Hopkins University School of Medicine (protocol no. MO16M431).

Body composition analysis

Body composition of *Ctrp2* KO and WT mice (18 weeks old) was determined using a quantitative NMR instrument (Echo-MRI-100, Echo Medical Systems LLC) at the Johns Hopkins University School of Medicine mouse phenotyping core facility. Echo-MRI analyses measure total fat mass, lean mass, and water content.

Indirect calorimetry

Ctrp2 KO and WT mice fed an LFD or an HFD for 20 weeks were used for simultaneous assessments of daily body weight change, food intake (corrected for spillage), physical activity, and whole-body metabolic profiling in an open flow indirect calorimeter (Comprehensive Laboratory Animal Monitoring System (CLAMS), Columbus Instruments). Data were collected for 3 days to confirm that mice were acclimated to the calorimetry chambers (indicated by stable body weights, food intake, and diurnal metabolic patterns), and data were analyzed from the fourth day onward. Rates of oxygen consumption ($\dot{V}_{O2}$) and carbon dioxide production ($\dot{V}_{CO2}$) in each chamber were measured throughout the study. Respiratory exchange ratio (RER = $\dot{V}_{CO2}/\dot{V}_{O2}$) was calculated by CLAMS software (version 4.02) to estimate the relative oxidation of carbohydrates (RER = 1.0) *versus* fats (RER = 0.7), not accounting for protein oxidation. Energy expenditure (EE) was calculated as EE = $\dot{V}_{O2} \times (3.815 + (1.232 \times \text{RER}))$. Physical activity was measured by IR beam breaks in the metabolic chamber. Average metabolic values were calculated per subject and averaged across subjects for statistical analysis.

Histological analysis of adipose tissue and liver

eWAT, iWAT, and liver from WT and KO mice (40 weeks old, fasted for 4 h) were removed and weighed after the mice were anesthetized with isoflurane. Formalin-fixed, paraffin-embedded tissues were stained with H&E at the Johns Hopkins University School of Medicine Reference Histology Laboratory. Images were captured with an AxioPlan upright microscope and an AxioCam color CCD camera (Carl Zeiss Microscopy).

RNA isolation and real-time PCR

Total RNA was isolated from tissue using TRIzol® Reagent and 2 μg of RNA was reverse-transcribed using GoScript™ Reverse Transcriptase (Promega). 1 ng/μl of cDNA from each sample was used in real-time PCR analysis using SYBR Green PCR Master Mix on a CFX Connect™ system (Bio-Rad). Results were analyzed using the $2^{-\Delta\Delta CT}$ method (53). Primer sequences are listed in Table 1.

Western blot analysis

Mouse tissues were homogenized in lysis buffer (20 mM Tris-HCl, 150 mM NaCl, 1 mM EDTA, 0.5% Nonidet P-40, and 10% glycerol) containing PhosSTOP phosphatase inhibitor mixture (Roche Applied Science) and Protease Inhibitor mixture

(Sigma). After the protein concentration was determined using Bradford reagent (Sigma), tissue lysates were used for Western blot analyses using anti-ATGL (1:1000, Cell Signaling Technology, no. 2138), anti-HSL (1:1000, Cell Signaling Technology, no. 4107), anti-MGL (1:500, Thermo Fisher Scientific, no. PA5–27915), anti–p-PKA substrates (1:1000, Cell Signaling Technology, no. 9621), and anti–β-actin (1:3000, Sigma, no. A1978) antibodies. Band intensities in blot images were quantified using ImageJ software (National Institutes of Health).

3T3-L1 adipocyte cell culture

Mouse 3T3-L1 cells were cultured in DMEM (Invitrogen) supplemented with 10% FBS and penicillin/streptomycin (Thermo Fisher Scientific). 2 days after cells reached confluence, adipocyte differentiation was induced with DMEM supplemented with 0.5 mM methylisobutylxanthine, 1 μM dexamethasone, and 4 μg/ml insulin for 3 days, followed by 4 μg/ml insulin for an additional 2 days. Cells were then maintained in DMEM with 10% FBS for an additional 3 days, by which time more than 90% of the cells had differentiated into mature adipocytes laden with lipid droplets. Recombinant full-length mouse CTRP2, containing a C-terminal FLAG epitope tag (DYKDDDDK), was produced in suspension HEK 293 cells at the Johns Hopkins Eukaryotic Tissue Culture Facility. Supernatants from transfected cells were subjected to affinity chromatography using an anti-FLAG M2 affinity gel (Sigma) according to the manufacturer's protocol. Purified protein was dialyzed against 20 mM HEPES (pH 8.0) containing 135 mM NaCl and concentrated with a 10 kDa cutoff Amicon Ultra-15 centrifugal filter unit (Millipore). Protein concentration was determined using Bradford reagent (Sigma) and samples were aliquoted and stored at −80 °C. For the lipolysis assay, adipocytes were treated with vehicle or CTRP2 (5 and 10 μg/ml) in DMEM with 0.2% BSA for 24 h. Then, cells were preincubated for 1 h with forskolin (10 μM) in the presence of triacsin C (5 μM) in DMEM (1 g/liter glucose) with 2% fatty acid–free BSA, and the incubation medium was replaced with fresh medium for 1 h. FFA content of the medium was determined using a Wako kit (Wako Chemicals) and normalized to the protein content of the cell lysate.

Plasma analysis

Tail vein or lateral saphenous vein blood samples were collected using Microvette® Lithium-Heparin coated capillary tubes. Blood was centrifuged for 10 min at 10,000 × *g*. Plasma samples were stored at −80 °C. FFAs and glycerol were measured using a Wako kit (Wako Chemicals) and Glycerol Assay Kit (Sigma), respectively. Plasma TG and cholesterol were measured using an Infinity™ kit (Thermo Fisher Scientific). For *in vivo* lipolysis, WT and KO mice were injected intraperitoneally (i.p.) with β_3-adrenergic receptor agonist CL316243 (Santa Cruz Biotechnology, no. SC203895) (1 mg/kg body weight (BW)) after 2 h of fasting in the morning. Blood was collected before and 15 min after injection. For FPLC, plasma collected from overnight-fasted mice was pooled (n = 4/group) and sent to the Mouse Metabolism Core at Baylor College of Medicine for FPLC separation and TG and cholesterol measurement. For LPL activity, plasma was collected from overnight-fasted mice 5 min after retro-orbital injection of 300 units/kg heparin, and then LPL and hepatic lipase activity were determined by LPL activity assay kit (BioVision).

Liver and fecal TG and cholesterol measurements

After liver tissue (~50 mg) was sonicated in 0.5-ml solution (5% Triton X-100 in water), the samples were slowly heated to 95 °C in a water bath until the Triton X-100 solution became cloudy and then cooled down to room temperature. The heating was repeated one more time to solubilize all TG. TG and cholesterol were measured using an Infinity™ kit (Thermo Fisher Scientific) after the samples were centrifuged at 20,000 × *g* for 2 min to remove any insoluble material and diluted 10-fold with dH_2O for measurement. For the analysis of fecal lipids, feces were collected from mice housed individually over a 24-h period, cleaned, and dried for 1 h at 70 °C. 100 mg aliquots were added to 500 μl saline and homogenized. Then, 200 μl of sample was incubated with 1 ml of chloroform-methanol (2:1) for 30 min at 60 °C with constant agitation and centrifuged for 10 min at 1000 × *g*. The lower chloroform phase was then transferred to a new tube, and the sample was evaporated to dryness. Samples were then resuspended in 500 μl 1% Triton X-100 in pure chloroform, evaporated to dryness, and finally resuspended in 500 μl of water. TG and cholesterol were measured using an Infinity™ kit (Thermo Fisher Scientific) using standards diluted with 1% Triton X-100 in water.

Glucose and insulin tolerance tests

LFD-fed *Ctrp2* KO male mice and WT littermates (22 weeks old) were subjected to intraperitoneal glucose tolerance tests (GTT) and insulin tolerance tests (ITT). For GTT, mice were fasted overnight before injection with glucose (1 g/kg BW). For ITT, food was removed 2 h before insulin injection (1 units/kg BW). Blood glucose was measured at the indicated time points using a glucometer (BD Pharmingen).

Lipid tolerance test

For OFTT, overnight-fasted mice were given an olive oil gavage (5 ml/kg BW) and blood was collected for TG measurement. For intraperitoneal fat tolerance testing, overnight-fasted mice were injected i.p. with 5 ml/kg BW of 20% (v/v) emulsified intralipid (Sigma), and blood was collected for TG measurement. To measure hepatic TG production, overnight-fasted mice were injected with 1 g/kg BW poloxamer 407 and blood was collected at the indicated time points.

Metabolomic analysis

Liver samples from LFD-fed WT and KO male mice were sent to Metabolon, Inc. (Durham, NC) for metabolomic profiling analysis as described previously (54).

Statistical analysis

Spearman's correlation coefficient analysis was used to analyze the associations between adipose expression of *CTRP2* and BMI. Kruskal-Wallis analysis of variance with pairwise comparisons was used to determine differences among the three groups (lean, obese without T2D, and obese with T2D). Two-way analysis of variance (ANOVA) was used to compare differ-

ences in body weight over time, energy expenditure, and lipid/glucose/insulin tolerance tests between WT and KO mice. Other comparisons were made using either a two-tailed Student's *t* test for two groups or one-way ANOVA for multiple groups. Values are reported as mean ± S.E. $p < 0.05$ was considered statistically significant.

Author contributions—X. L. and G. W. W. conceptualization; X. L. and G. W. W. data curation; X. L. and G. W. W. formal analysis; X. L. and G. W. W. supervision; X. L. and G. W. W. funding acquisition; X. L. and G. W. W. validation; X. L. and G. W. W. investigation; X. L. and G. W. W. methodology; X. L. and G. W. W. writing-original draft; X. L. and G. W. W. project administration; X. L. and G. W. W. writing-review and editing.

Acknowledgment—We thank Susan Aja for help with indirect calorimetry.

References

1. Attie, A. D., and Scherer, P. E. (2009) Adipocyte metabolism and obesity. *J. Lipid Res.* **50,** (suppl.) S395–S399 CrossRef Medline
2. Rosen, E. D., and Spiegelman, B. M. (2006) Adipocytes as regulators of energy balance and glucose homeostasis. *Nature* **444,** 847–853 CrossRef Medline
3. Scherer, P. E. (2006) Adipose tissue: From lipid storage compartment to endocrine organ. *Diabetes* **55,** 1537–1545 CrossRef Medline
4. Rosen, E. D., and Spiegelman, B. M. (2014) What we talk about when we talk about fat. *Cell* **156,** 20–44 CrossRef Medline
5. Ahima, R. S., and Lazar, M. A. (2008) Adipokines and the peripheral and neural control of energy balance. *Mol. Endocrinol.* **22,** 1023–1031 CrossRef Medline
6. Ouchi, N., Parker, J. L., Lugus, J. J., and Walsh, K. (2011) Adipokines in inflammation and metabolic disease. *Nat. Rev. Immunol.* **11,** 85–97 CrossRef Medline
7. Seldin, M. M., Peterson, J. M., Byerly, M. S., Wei, Z., and Wong, G. W. (2012) Myonectin (CTRP15), a novel myokine that links skeletal muscle to systemic lipid homeostasis. *J. Biol. Chem.* **287,** 11968–11980 CrossRef Medline
8. Wei, Z., Peterson, J. M., Lei, X., Cebotaru, L., Wolfgang, M. J., Baldeviano, G. C., and Wong, G. W. (2012) C1q/TNF-related protein-12 (CTRP12), a novel adipokine that improves insulin sensitivity and glycemic control in mouse models of obesity and diabetes. *J. Biol. Chem.* **287,** 10301–10315 CrossRef Medline
9. Wei, Z., Peterson, J. M., and Wong, G. W. (2011) Metabolic regulation by C1q/TNF-related protein-13 (CTRP13): Activation of AMP-activated protein kinase and suppression of fatty acid-induced JNK signaling. *J. Biol. Chem.* **286,** 15652–15665 CrossRef Medline
10. Wei, Z., Seldin, M. M., Natarajan, N., Djemal, D. C., Peterson, J. M., and Wong, G. W. (2013) C1q/tumor necrosis factor-related protein 11 (CTRP11), a novel adipose stroma-derived regulator of adipogenesis. *J. Biol. Chem.* **288,** 10214–10229 CrossRef Medline
11. Wong, G. W., Krawczyk, S. A., Kitidis-Mitrokostas, C., Ge, G., Spooner, E., Hug, C., Gimeno, R., and Lodish, H. F. (2009) Identification and characterization of CTRP9, a novel secreted glycoprotein, from adipose tissue that reduces serum glucose in mice and forms heterotrimers with adiponectin. *FASEB J.* **23,** 241–258 CrossRef Medline
12. Wong, G. W., Krawczyk, S. A., Kitidis-Mitrokostas, C., Revett, T., Gimeno, R., and Lodish, H. F. (2008) Molecular, biochemical and functional characterizations of C1q/TNF family members: Adipose-tissue-selective expression patterns, regulation by PPAR-gamma agonist, cysteine-mediated oligomerizations, combinatorial associations and metabolic functions. *Biochem. J.* **416,** 161–177 CrossRef Medline
13. Wong, G. W., Wang, J., Hug, C., Tsao, T. S., and Lodish, H. F. (2004) A family of Acrp30/adiponectin structural and functional paralogs. *Proc. Natl. Acad. Sci. U.S.A.* **101,** 10302–10307 CrossRef Medline
14. Seldin, M. M., Tan, S. Y., and Wong, G. W. (2014) Metabolic function of the CTRP family of hormones. *Rev. Endocr. Metab. Disord.* **15,** 111–123 CrossRef Medline
15. Kishore, U., Gaboriaud, C., Waters, P., Shrive, A. K., Greenhough, T. J., Reid, K. B., Sim, R. B., and Arlaud, G. J. (2004) C1q and tumor necrosis factor superfamily: Modularity and versatility. *Trends Immunol.* **25,** 551–561 CrossRef Medline
16. Lei, X., Rodriguez, S., Petersen, P. S., Seldin, M. M., Bowman, C. E., Wolfgang, M. J., and Wong, G. W. (2016) Loss of CTRP5 improves insulin action and hepatic steatosis. *Am. J. Physiol. Endocrinol. Metab.* **310,** E1036–E1052 CrossRef Medline
17. Lei, X., Seldin, M. M., Little, H. C., Choy, N., Klonisch, T., and Wong, G. W. (2017) C1q/TNF-related protein 6 (CTRP6) links obesity to adipose tissue inflammation and insulin resistance. *J. Biol. Chem.* **292,** 14836–14850 CrossRef Medline
18. Petersen, P. S., Lei, X., Wolf, R. M., Rodriguez, S., Tan, S. Y., Little, H. C., Schweitzer, M. A., Magnuson, T. H., Steele, K. E., and Wong, G. W. (2017) CTRP7 deletion attenuates obesity-linked glucose intolerance, adipose tissue inflammation, and hepatic stress. *Am. J. Physiol. Endocrinol. Metab.* **312,** E309–E325 CrossRef Medline
19. Peterson, J. M., Aja, S., Wei, Z., and Wong, G. W. (2012) C1q/TNF-related protein-1 (CTRP1) enhances fatty acid oxidation via AMPK activation and ACC inhibition. *J. Biol. Chem.* **287,** 1576–1587 CrossRef Medline
20. Peterson, J. M., Seldin, M. M., Wei, Z., Aja, S., and Wong, G. W. (2013) CTRP3 attenuates diet-induced hepatic steatosis by regulating triglyceride metabolism. *Am. J. Physiol. Gastrointest. Liver Physiol.* **305,** G214–G224 CrossRef Medline
21. Peterson, J. M., Wei, Z., Seldin, M. M., Byerly, M. S., Aja, S., and Wong, G. W. (2013) CTRP9 transgenic mice are protected from diet-induced obesity and metabolic dysfunction. *Am. J. Physiol. Regul. Integr. Comp. Physiol.* **305,** R522–R533 CrossRef Medline
22. Peterson, J. M., Wei, Z., and Wong, G. W. (2010) C1q/TNF-related protein-3 (CTRP3), a novel adipokine that regulates hepatic glucose output. *J. Biol. Chem.* **285,** 39691–39701 CrossRef Medline
23. Rodriguez, S., Lei, X., Petersen, P. S., Tan, S. Y., Little, H. C., and Wong, G. W. (2016) Loss of CTRP1 disrupts glucose and lipid homeostasis. *Am. J. Physiol. Endocrinol. Metab.* **311,** E678–E697 CrossRef Medline
24. Tan, S. Y., Little, H. C., Lei, X., Li, S., Rodriguez, S., and Wong, G. W. (2016) Partial deficiency of CTRP12 alters hepatic lipid metabolism. *Physiol. Genomics* **48,** 936–949 CrossRef Medline
25. Wei, Z., Lei, X., Petersen, P. S., Aja, S., and Wong, G. W. (2014) Targeted deletion of C1q/TNF-related protein 9 increases food intake, decreases insulin sensitivity, and promotes hepatic steatosis in mice. *Am. J. Physiol. Endocrinol. Metab.* **306,** E779–E790 CrossRef Medline
26. Wolf, R. M., Lei, X., Yang, Z. C., Nyandjo, M., Tan, S. Y., and Wong, G. W. (2016) CTRP3 deficiency reduces liver size and alters IL-6 and TGFβ levels in obese mice. *Am. J. Physiol. Endocrinol. Metab.* **310,** E332–E345 CrossRef Medline
27. Enomoto, T., Ohashi, K., Shibata, R., Higuchi, A., Maruyama, S., Izumiya, Y., Walsh, K., Murohara, T., and Ouchi, N. (2011) Adipolin/C1qdc2/CTRP12 functions as an adipokine that improves glucose metabolism. *J. Biol. Chem.* **286,** 34552–34558 CrossRef Medline
28. Han, S., Park, J. S., Lee, S., Jeong, A. L., Oh, K. S., Ka, H. I., Choi, H. J., Son, W. C., Lee, W. Y., Oh, S. J., Lim, J. S., Lee, M. S., and Yang, Y. (2016) CTRP1 protects against diet-induced hyperglycemia by enhancing glycolysis and fatty acid oxidation. *J. Nutr. Biochem.* **27,** 43–52 CrossRef Medline
29. Little, H. C., Rodriguez, S., Lei, X., Tan, S. Y., Stewart, A. N., Sahagun, A., Sarver, D. C., and Wong, G. W. (2019) Myonectin deletion promotes adipose fat storage and reduces liver steatosis. *FASEB J.* **33,** 8666–8687 CrossRef Medline
30. Peterson, J. M., Seldin, M. M., Tan, S. Y., and Wong, G. W. (2014) CTRP2 overexpression improves insulin and lipid tolerance in diet-induced obese mice. *PLoS One* **9,** e88535 CrossRef Medline
31. Rohrbach, S., Aurich, A. C., Li, L., and Niemann, B. (2007) Age-associated loss in adiponectin-activation by caloric restriction: lack of compensation by enhanced inducibility of adiponectin paralogs CTRP2 and CTRP7. *Mol. Cell. Endocrinol.* **277,** 26–34 CrossRef Medline

32. Duncan, R. E., Ahmadian, M., Jaworski, K., Sarkadi-Nagy, E., and Sul, H. S. (2007) Regulation of lipolysis in adipocytes. *Annu. Rev. Nutr.* **27,** 79–101 CrossRef Medline
33. Litosch, I., Hudson, T. H., Mills, I., Li, S. Y., and Fain, J. N. (1982) Forskolin as an activator of cyclic AMP accumulation and lipolysis in rat adipocytes. *Mol. Pharmacol.* **22,** 109–115 Medline
34. Millar, J. S., Cromley, D. A., McCoy, M. G., Rader, D. J., and Billheimer, J. T. (2005) Determining hepatic triglyceride production in mice: comparison of poloxamer 407 with Triton WR-1339. *J. Lipid Res.* **46,** 2023–2028 CrossRef Medline
35. Hollenberg, C. H., Raben, M. S., and Astwood, E. B. (1961) The lipolytic response to corticotropin. *Endocrinology* **68,** 589–598 CrossRef Medline
36. Rizack, M. A. (1964) Activation of an epinephrine-sensitive lipolytic activity from adipose tissue by adenosine 3′,5′-phosphate. *J. Biol. Chem.* **239,** 392–395 Medline
37. Vaughan, M., Berger, J. E., and Steinberg, D. (1964) Hormone-sensitive lipase and monoglyceride lipase activities in adipose tissue. *J. Biol. Chem.* **239,** 401–409 Medline
38. Kim, J. Y., Tillison, K., Lee, J. H., Rearick, D. A., and Smas, C. M. (2006) The adipose tissue triglyceride lipase ATGL/PNPLA2 is down-regulated by insulin and TNF-α in 3T3-L1 adipocytes and is a target for transactivation by PPARγ. *Am. J. Physiol. Endocrinol. Metab.* **291,** E115–E127 CrossRef Medline
39. Liu, L. F., Purushotham, A., Wendel, A. A., Koba, K., DeIuliis, J., Lee, K., and Belury, M. A. (2009) Regulation of adipose triglyceride lipase by rosiglitazone. *Diabetes Obes. Metab.* **11,** 131–142 CrossRef Medline
40. Villena, J. A., Roy, S., Sarkadi-Nagy, E., Kim, K. H., and Sul, H. S. (2004) Desnutrin, an adipocyte gene encoding a novel patatin domain-containing protein, is induced by fasting and glucocorticoids: Ectopic expression of desnutrin increases triglyceride hydrolysis. *J. Biol. Chem.* **279,** 47066–47075 CrossRef Medline
41. Nielsen, T. S., Jessen, N., Jørgensen, J. O., Møller, N., and Lund, S. (2014) Dissecting adipose tissue lipolysis: Molecular regulation and implications for metabolic disease. *J. Mol. Endocrinol.* **52,** R199–R222 CrossRef Medline
42. Nielsen, S., Guo, Z., Johnson, C. M., Hensrud, D. D., and Jensen, M. D. (2004) Splanchnic lipolysis in human obesity. *J. Clin. Invest.* **113,** 1582–1588 CrossRef Medline
43. Wedellová, Z., Dietrich, J., Siklová-Vítková, M., Kološtová, K., Kováčiková, M., Dušková, M., Brož, J., Vedral, T., Stich, V., and Polák, J. (2011) Adiponectin inhibits spontaneous and catecholamine-induced lipolysis in human adipocytes of non-obese subjects through AMPK-dependent mechanisms. *Physiol. Res.* **60,** 139–148 Medline
44. Qiao, L., Kinney, B., Schaack, J., and Shao, J. (2011) Adiponectin inhibits lipolysis in mouse adipocytes. *Diabetes* **60,** 1519–1527 CrossRef Medline
45. Nakajima, K., Nakano, T., Tokita, Y., Nagamine, T., Inazu, A., Kobayashi, J., Mabuchi, H., Stanhope, K. L., Havel, P. J., Okazaki, M., Ai, M., and Tanaka, A. (2011) Postprandial lipoprotein metabolism: VLDL vs chylomicrons. *Clin. Chim. Acta* **412,** 1306–1318 CrossRef Medline
46. Tsai, M. Y., Georgopoulos, A., Otvos, J. D., Ordovas, J. M., Hanson, N. Q., Peacock, J. M., and Arnett, D. K. (2004) Comparison of ultracentrifugation and nuclear magnetic resonance spectroscopy in the quantification of triglyceride-rich lipoproteins after an oral fat load. *Clin. Chem.* **50,** 1201–1204 CrossRef Medline
47. Wang, H., and Eckel, R. H. (2009) Lipoprotein lipase: from gene to obesity. *Am. J. Physiol. Endocrinol. Metab.* **297,** E271–E288 CrossRef Medline
48. Dietschy, J. M., and Turley, S. D. (2002) Control of cholesterol turnover in the mouse. *J. Biol. Chem.* **277,** 3801–3804 CrossRef Medline
49. Sundaram, M., and Yao, Z. (2010) Recent progress in understanding protein and lipid factors affecting hepatic VLDL assembly and secretion. *Nutr. Metab.* **7,** 35 CrossRef Medline
50. Gruffat, D., Durand, D., Graulet, B., and Bauchart, D. (1996) Regulation of VLDL synthesis and secretion in the liver. *Reprod. Nutr. Dev.* **36,** 375–389 CrossRef Medline
51. Yao, Z. M., and Vance, D. E. (1988) The active synthesis of phosphatidylcholine is required for very low-density lipoprotein secretion from rat hepatocytes. *J. Biol. Chem.* **263,** 2998–3004 Medline
52. Nishimaki-Mogami, T., Yao, Z., and Fujimori, K. (2002) Inhibition of phosphatidylcholine synthesis via the phosphatidylethanolamine methylation pathway impairs incorporation of bulk lipids into VLDL in cultured rat hepatocytes. *J. Lipid Res.* **43,** 1035–1045 CrossRef Medline
53. Schmittgen, T. D., and Livak, K. J. (2008) Analyzing real-time PCR data by the comparative C(T) method. *Nat. Protoc.* **3,** 1101–1108 CrossRef Medline
54. Reitman, Z. J., Jin, G., Karoly, E. D., Spasojevic, I., Yang, J., Kinzler, K. W., He, Y., Bigner, D. D., Vogelstein, B., and Yan, H. (2011) Profiling the effects of isocitrate dehydrogenase 1 and 2 mutations on the cellular metabolome. *Proc. Natl. Acad. Sci. U.S.A.* **108,** 3270–3275 CrossRef Medline